Available online at https://link.springer.com/journal/42241
http://www.jhydrodynamics.com
Journal of Hydrodynamics, 2022, 34(4): 756-766
https://doi.org/10.1007/s42241-022-0061-0

Numerical simulation and scaling analysis of elasticity-induced lift force in a viscoelastic fluid between confining surfaces

Xin Zhao[1], Chao Wei[2*]
1. *The State Key Laboratory of Nonlinear Mechanics, Institute of Mechanics, Chinese Academy of Sciences, Beijing 100190, China*
2. *Science and Technology on Vehicle Transmission Laboratory, Beijing Institute of Technology, Beijing 100081, China*

(Received December 24, 2021, Revised June 28, 2022, Accepted July 3, 2022, Published online September 7, 2022)

Abstract: How to accurately characterize the lift force on the particles near the solid surfaces is an ongoing challenge in fluid mechanics and microfluidic techniques, especially in a complex system with viscoelastic fluid or/and soft surface that is commonly encountered in a biological system. The motions of the particles in vicinity of a surface can be simplified to be a rigid cylinder surrounded by the viscoelastic fluid moving along a substrate which can be rigid or soft according to different cases. In such an inertial free system with a wide range of Weissenberg number ($Wi < 5.00$, representing the ratio of the elastic force to the viscous force), firstly we numerically evaluate the influence of the systematic parameters, including the polymer viscosity, the geometry and Wi, on the net normal force for a cylinder closely moving along a rigid substrate, and the elasticity-induced lift force in a scaled form . It is shown that a strong shear arises in the viscoelastic confinement between the moving cylinder and the rigid substrate, it leads to the asymmetry of the first normal stress distribution around the cylinder, and thus the lift force. Then, the influence of a soft substrate on the lift force is considered, and we find that the lift force induced by the viscoelastic fluid always dominates in magnitude over that induced by the soft substrate deformation. This work provides a reliable scaling that can be utilized to quantify the elasticity-induced lift force on the particles in a viscoelastic system, such as the micro- and nanofluidic systems in biological applications.

Key words: Viscoelastic fluid, scaling expression, computational fluid dynamics, lift force

Introduction

The motion of the particles in a lubrication flow near a boundary is ubiquitous and of a great significance in various natural and industrial processes[1-6]. The hydrodynamic interaction between the particle and the boundary is fundamental to understand the particle transport, especially, the non-intuitive lateral migration of the particle perpendicular to the flow direction[7-9]. The lateral migration in the viscous shear flows with relatively high Reynolds number (Re) is attributed to the inertial effect, which produces a non-zero net normal force, so-called the lift force, to push the particles away from the boundary. Such lateral migration of the particles in the channel flow has been widely applied in various fields from the well-known macroscale "tubular pinch effect"[10] to the flow focusing in microfluidics[11].

New challenges arise in biological and physiological flows[12], or in the manipulation of nanoscale particles by lab-on-a-chip devices[13]. For instance, it was found that the platelets and the red blood cells (RBCs) manifested different lateral migration behaviors in the slow blood flow within a highly constricted arteriole[14], the lift force was employed to separate nanoscale exosomes from extracellular vesicles in biological complex fluids[13]. Different from the aforementioned inertial mechanism, the interactions of the ubiquitous viscoelastic fluids in biological systems with the external shear due to the elasticity and the shear-thinning, completely alter the lateral migration dynamics of the particles. The Weissenberg number (Wi) is introduced to describe the ratio between the elastic force and the viscous force as representing the recoverable strain in the fluid[15]. In micro- and nanofluidic systems, the Reynolds number is often smaller than unity, leading to a negligible inertia-induced lift force. Whereas, if surrounded by a viscoelastic flow, the elasticity-

Project supported by the National Natural Science Foundation of China (Grant No. 51875039).
Biography: Xin Zhao (1991-), Female, Ph. D.,
E-mail: pekingbit@163.com
Corresponding author: Chao Wei,
E-mail: wei_chao_bit @163.com

induced net stress may lift the particles away from the boundary[16-19]. This elasticity-induced lift becomes a new and significant mechanism in the low Reynolds number viscoelastic flow, where the elasticity number El (the ratio of the elastic force to the inertial force) could be much larger than unity.

However, existing investigations based on the viscoelastic constitutive and the Navier-Stokes equation mainly focused on the flow profile in the unbounded domain[20-23]. For example, Fetecau discussed the exact solution to the flows of an Oldroyd-B fluid above infinite half space and in infinite cylindrical domains[21-23]. With respect to the confined flow interacted between the particle and the substrate, the motion of a sphere sheared in the viscoelastic fluid is simply estimated based on the difference of the averaged first normal stress at upper and lower hemispheres[24]. It clarified the mechanism of the normal stress induced by the shear but indiscriminatingly simplified the contributions of physical and geometry factors in different systems. There appears no consensus of the theoretical expression of the lift force due to the elastic contribution so far.

Recently, it has been demonstrated that the elastic deformation of the soft surface can also induce the lift force between the substrate and the moving surface due to its influence on the pressure distribution in the gap region[25-31]. This elasto-hydrodynamic lift has been considered as a fundamental issue in many biophysical problems, such as the RBC cell motion in capillaries[14] and the biolubrications[28]. In the past two decades, the mechanism of the elasto-hydrodynamic lift in the viscous fluid was elaborately investigated theoretically[25-27], experimentally[29-31]. However, a more realistic consideration of the coupling between the soft substrate and the viscoelastic fluid is still required.

In this study, the numerical simulation and the scaling analysis are made for the lift force induced by the viscoelastic confinement between a moving cylinder and a substrate, to clarify the contributions of the viscoelastic fluid and the soft boundary. Our study focuses on the flow in the small Reynolds number regime while the Weissenberg number covers a wide range up to 5.00, demonstrating that a strong lift force comes from a large elastic effect in a viscoelastic fluid. Firstly, a theoretical expression is deduced for the elasticity-induced lift force between the rigid substrates based on the scaling analysis and the numerical simulation. It is demonstrated that a strong lift force might come from a large elastic effect of the viscoelastic fluid. Secondly, the presence of a soft surface is further considered, with the elasticity modulus varying in a wide range from kPa to MPa in the simulation according to the biological softness. It is shown that the lift force in the viscoelastic fluid can always be of a magnitude dominant over the elasto-hydrodynamic lift force in the viscous fluid with the coexistence of the soft substrate and the viscoelastic fluid in the micro- and nanofluidics. Our findings provide insights for understanding the non-intuitive migration behaviors of the particles in various biological and physiological applications.

1. Modelling

1.1 *Governing equations*

We consider a micro particle of radius R immersed in a polymer solution near a solid substrate, moving at a certain velocity. The particle is simplified as a rigid cylinder immersed in the viscoelastic fluid sliding or rotating over the substrate, as indicated in Fig. 1. Here H_0 is the minimum distance between the cylinder and the substrate, U and ωR are the translational and rotational velocities of the cylinder. The motion of the cylinder will be set as the velocity boundary condition during the calculation. For a buoyance force and gravity free system, the time-dependent governing equations of an incompressible viscoelastic fluid are as follows[32-33]

$$\nabla \cdot \boldsymbol{U} = 0, \quad \rho\left[\frac{\partial \boldsymbol{U}}{\partial T} + (\boldsymbol{U}\cdot\nabla)\boldsymbol{U}\right] = \nabla\cdot[-P\mathbf{I} + \mu_{s0}(\nabla\boldsymbol{U} + \nabla\boldsymbol{U}^{\mathrm{T}}) + \boldsymbol{S}] \tag{1}$$

where $\boldsymbol{U}$ is the velocity tensor in the flow domain, $\boldsymbol{S}$ is the elastic tensor in the viscoelastic constitutive equation, ρ is the density of the solution, P is the pressure field and μ_{s0} is the viscosity of the solvent. The no-slip boundary condition is applied on all solid surfaces. The velocity boundary condition of the cylinder should be given specially based on the descryption of the translational and rotational velocities of the cylinder.

The Oldroyb-B model[34], which is commonly used in the constitutive modeling of the viscoelastic fluid, is chosen to analyze both the viscoelastic effect on the flow and the force acting on the cylinder. The constitutive equation of the Oldroyb-B fluid is

$$\boldsymbol{S} + \lambda_1 \frac{\mathrm{D}}{\mathrm{D}T}\boldsymbol{S} = \mu_{p0}(\nabla\boldsymbol{U} + \nabla\boldsymbol{U}^{\mathrm{T}}) \tag{2}$$

where λ_1 is the relaxation time of the viscoelastic solution, μ_{p0} is the viscosity of the viscoelastic component like the polymer, $\mathrm{D}/\mathrm{D}T$ denotes the upper convected time derivative and

$$\frac{\mathrm{D}}{\mathrm{D}T}\boldsymbol{S}=\frac{\partial}{\partial T}\boldsymbol{S}+(\boldsymbol{U}\cdot\nabla)\boldsymbol{S}-[(\nabla\boldsymbol{U})\boldsymbol{S}+\boldsymbol{S}(\nabla\boldsymbol{U})^{\mathrm{T}}]$$

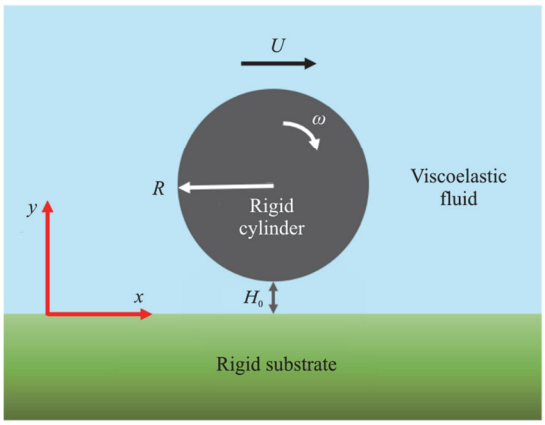

Fig. 1 (Color online) A rigid cylinder moves through a viscoelastic solution above a solid substrate

The time-dependent governing equations in a dimensionless format are as follows:

$$\nabla\cdot\boldsymbol{u}=0,$$

$$Re\left[\frac{\partial\boldsymbol{u}}{\partial t}+(\boldsymbol{u}\cdot\nabla)\boldsymbol{u}\right]=$$

$$\nabla\cdot\left\{-p\mathbf{I}+\mu_s(\nabla\boldsymbol{u}+\nabla\boldsymbol{u}^{\mathrm{T}})+\mu_p(\nabla\boldsymbol{u}+\nabla\boldsymbol{u}^{\mathrm{T}})-\right.$$

$$\left.Wi\left\{\frac{\partial\boldsymbol{s}}{\partial t}(\boldsymbol{u}\cdot\nabla)\boldsymbol{s}-[(\nabla\boldsymbol{u})\boldsymbol{s}+\boldsymbol{s}(\nabla\boldsymbol{u})^{\mathrm{T}}\right\}\right. \tag{3}$$

with the dimensionless variables:

$$\boldsymbol{u}=\frac{\boldsymbol{U}}{U_0},\quad x=\frac{X}{L_0},\quad y=\frac{Y}{L_0},\quad \mu_p=\frac{\mu_{p0}}{\mu_{p0}+\mu_{s0}},$$

$$\mu_s=\frac{\mu_{s0}}{\mu_{p0}+\mu_{s0}},\quad Wi=\lambda_1\frac{U_0}{L_0},\quad Re=\frac{\rho U_0 L_0}{\mu_{p0}+\mu_{s0}},$$

$$p=P\frac{L_0}{(\mu_{p0}+\mu_{s0})U_0},\quad t=T\frac{U_0}{L_0},\quad \boldsymbol{s}=\boldsymbol{S}\frac{L_0}{U_0(\mu_{p0}+\mu_{s0})}$$

Note that in the above equations, the left hand side is the dimensionless variables, and the right hand side is the dimensional variables.

Before further discussing the above control equations, the rationality of them is tested in a simple shear flow, and the numerical results fit well with the analytical results, as presented in the Appendix.

1.2 *Decomposing of the governing equations*

In micro- and nanofluidics, the small inertia leads to a very small Reynolds number ($Re\ll1$). Moreover, the polymer relaxation time is in a scale of $\sim\lambda_1$, and thus the time-dependent behavior of the fluid occurs at the distance of $\sim U\lambda_1$ (usually smaller than μm) away from the cylinder. The velocity field fluctuation region is in a scale of $(RH_0)^{0.5}$, indicating that the time-dependent behavior of the polymer disappears before the particle is in the steady motion. Therefore, the inertia term and the time derivative of the elastic tensor can be neglected, and we simplify the governing equation by neglecting the inertial and time-dependent terms in Eq. (3)

$$\nabla\cdot\left\{p\mathbf{I}+\mu_s(\nabla\boldsymbol{u}+\nabla\boldsymbol{u}^{\mathrm{T}})+\mu_p(\nabla\boldsymbol{u}+\nabla\boldsymbol{u}^{\mathrm{T}})-\right.$$

$$\left.Wi\{(\boldsymbol{u}\cdot\nabla)\boldsymbol{s}-[(\nabla\boldsymbol{u})\boldsymbol{s}+\boldsymbol{s}(\nabla\boldsymbol{u})^{\mathrm{T}}]\}\right\}=0 \tag{4}$$

We further decompose the dimensionless pressure p into two components ($p=p_v+p_e$), and we name them as the viscous component p_v and the elastic component p_e. Therefore, Eq. (4) can be written as follows

$$\nabla\cdot[-p_v\mathbf{I}+\mu_s(\nabla\boldsymbol{u}+\nabla\boldsymbol{u}^{\mathrm{T}})+\mu_p(\nabla\boldsymbol{u}+\nabla\boldsymbol{u}^{\mathrm{T}})]+$$

$$\nabla\cdot\{-p_e\mathbf{I}-Wi\{(\boldsymbol{u}\cdot\nabla)\boldsymbol{s}-$$

$$[(\nabla\boldsymbol{u})\boldsymbol{s}+\mathbf{s}(\nabla\boldsymbol{u})^{\mathrm{T}}]\}\}=0 \tag{5}$$

To visualize the flow field, we conduct the simulation by using the Comsol Multiphysics 5.5. A Multifrontal Massively Parallel Sparse direct Solver is chosen as solver. The cylinder is fixed in an aqueous polymer solution with a solvent viscosity of 8.9 mPa·s under the ambient pressure at 298 K, and the substrate is moved translationally to produce the flow. Eqs. (1), (2) are solved in the numerical simulation with the sweeping parameters of Wi in the range from 0.1 to 1.0 and the polymer viscosity μ_{p0} in the range from 5 mPa·s to 20 mPa·s. The other system parameters are listed in Table 1. Two representatives of the velocity contour are shown in Fig. 2.

It can be seen in Fig. 2 that the velocity gradient in the confined gap between the lower hemisphere and the surface is significantly enhanced, leading to an asymmetry distribution of the shear stress around the cylinder. Within the simulated range of Wi, the velocity contour changes very slightly around the cylinder. The velocity contours in Fig. 2 are almost symmetric,

which is similar to those of the Stokes flow in symmetric geometry and boundary conditions. Thus, it is suggested that the term in the governing equation containing Wi has little effect on the velocity field. Based on this analysis, we can define the pressure component p_v to balance the viscous force of both the solvent and the polymer induced by the velocity gradient field, and the rest pressure p_e to balance the elastic force. Due to the weak correlation between Wi and the velocity field, Eq. (5) can be decomposed into one linear partial differential equation, which is the same as that for the Stokes flow Eq. (6a), and another non-linear partial differential equation (6b) as:

Table 1 Parameters of the simulations shown in Fig. 2

	Value
L_0 /μm	1.0
r	6
H_0 /μm	1.5
Viscosity of solvent, μ_{s0} /mPa·s	8.9
Viscosity of polymer, μ_{p0} /mPa·s	6.2
Velocity, $\boldsymbol{U}$ /(μm·s^{-1})	10

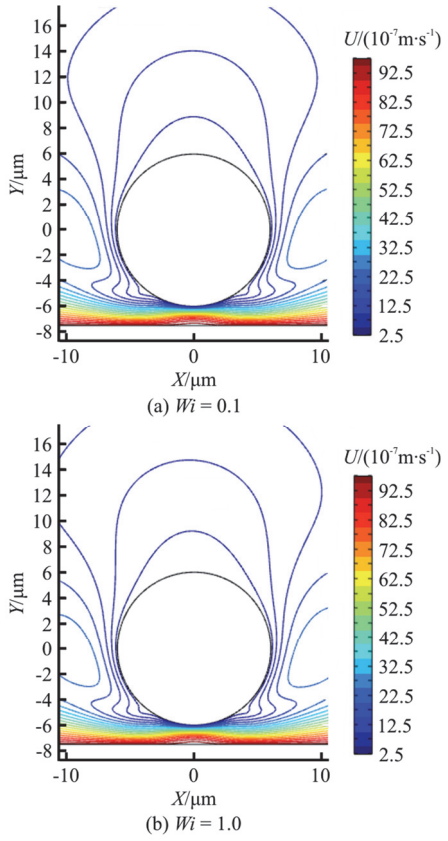

Fig. 2 (Color online) Velocity contours around a cylinder in a viscoelastic fluid

$$\nabla\cdot[-p_v\mathbf{I}+\mu_s(\nabla\boldsymbol{u}+\nabla\boldsymbol{u}^{\mathrm{T}})+\mu_p(\nabla\boldsymbol{u}+\nabla\boldsymbol{u}^{\mathrm{T}})]=0 \quad (6a)$$

$$\nabla\cdot\{-p_e\mathbf{I}-Wi\{(\boldsymbol{u}\cdot\nabla)\boldsymbol{s}-[(\nabla\boldsymbol{u})\boldsymbol{s}+\boldsymbol{s}(\nabla\boldsymbol{u})^{\mathrm{T}}]\}\}=0 \quad (6b)$$

2. Scaling expression of the elasticity-induced lift force

2.1 *Component analysis of elasticity-induced lift force between rigid surfaces*

The lift force on the particle includes the viscous stress and the polymer stress. And from Eq. (6a), p_v is responsible for the viscous stress. Similarly, from Eq. (6b), p_e is responsible for the polymer stress. The lift force acting on the cylinder is defined as the integral of the vertical component of the pressure p around the cylinder. With a small Re as investigated in our system, the pressure p_v contributed by the viscous shear is antisymmetric and does not produce a net lift force. Thus, the lift force in a viscoelastic fluid in the case of a small Re is produced only by the elasticity, eg., p_e, which arises from the upper convected time derivative in Eq. (6b). Then, the lift force is expressed as

$$f_{\mathrm{lift}}=\int_l p\cdot\boldsymbol{n}_y\mathrm{d}l=\int_l p_v\cdot\boldsymbol{n}_y\mathrm{d}l+\int_l p_e\cdot\boldsymbol{n}_y\mathrm{d}l=\int_l p_e\cdot\boldsymbol{n}_y\mathrm{d}l \quad (7)$$

Based on the decomposition in Section 1.2, the flow field can be calculated independently by using Eq. (6a) with the boundary conditions. The lift force can be further calculated based on the elastic tensor and the velocity field by using Eq. (6b).

However, in the following, the dominant force in the system will be found out by checking every component of the viscous and elastic stress tensors in Eq. (8), and then the lift force can be estimated according to the dominant force. The control equation in the array format, which should be satisfied in the whole domain and boundary, is as follows

$$\begin{bmatrix}\frac{1}{\partial x} & \frac{1}{\partial y}\end{bmatrix}\left\{\begin{bmatrix}-p & 0\\ 0 & -p\end{bmatrix}+\mu_s\begin{bmatrix}2\frac{\partial u}{\partial x} & \frac{\partial v}{\partial x}+\frac{\partial u}{\partial y}\\ \frac{\partial v}{\partial x}+\frac{\partial u}{\partial y} & 2\frac{\partial v}{\partial y}\end{bmatrix}+\begin{bmatrix}S_{xx} & S_{xy}\\ S_{yx} & S_{yy}\end{bmatrix}\right\}=0 \quad (8)$$

where u, v are the dimensionless velocity components in x, y directions. In the vicinity of the no-slip boundary, $u\sim 0$, $v\sim 0$. Thus, a simplified expression is obtained near the particle surface

$$\begin{bmatrix} \frac{1}{\partial x} & \frac{1}{\partial y} \end{bmatrix} \left\{ \begin{bmatrix} -p_v & 0 \\ 0 & -p_v \end{bmatrix} + (\mu_s + \mu_p) \begin{bmatrix} 0 & \frac{\partial u}{\partial y} \\ \frac{\partial u}{\partial y} & 2\frac{\partial v}{\partial y} \end{bmatrix} + \begin{bmatrix} -p_e & 0 \\ 0 & -p_e \end{bmatrix} + Wi \begin{bmatrix} 2\frac{\partial u}{\partial x} S_{xx} & \frac{\partial u}{\partial y} S_{yy} + \frac{\partial v}{\partial x} S_{xx} \\ \frac{\partial u}{\partial y} S_{yy} + \frac{\partial v}{\partial x} S_{xx} & 2\frac{\partial v}{\partial x} S_{yx} + \frac{\partial v}{\partial x} S_{xy} \end{bmatrix} \right\} \sim 0 \tag{9}$$

By comparing the order of magnitude of each component in the elastic tensor in the ranges of $Wi(0.1\text{-}1.0)$, the viscosity ratio μ_p (μ_{p0} = 5 mPa·s - 20 mPa·s), the term $(\partial u/\partial y)(\partial s_{xy}/\partial x)$ is the dominant component in Eq. (9). Comparison of the shear rate and the extracted curves of $(\partial u/\partial y)$ confirms that the main flow feature within the confinement is that of a plane shear flow and the main contribution to the shear rate comes from $(\partial u/\partial y)$. Similar to a plane shear flow, and with the consideration of the decomposition in Section 1.2, an estimation, $p_e \sim 2Wi\partial u/\partial y s_{xy}$, with $s_{xy} = \mu_p \partial u/\partial y$ leads to $p_e \sim 2Wi\mu_p(\partial u/\partial y)^2 \sim 2Wi\mu_p(u/h_0)^2 \sim s_{xx}$. In this way, the dimensionless lift force can be evaluated by summing up the first normal stress within the characterized region as

$$f_{\text{lift}} \sim \int_l s_{xx} \mathrm{d}l \sim 2Wi\mu_p \int_{-(2rh_0)^{0.5}/2}^{(2rh_0)^{0.5}/2} \left(\frac{u}{h_0 + x^2/2r} \right)^2 \mathrm{d}x \sim 2\Omega i \mu_p u^2 \frac{r^{0.5}}{h_0^{1.5}} \tag{10}$$

where $(2rh_0)^{0.5}$ is the dimensionless characteristic length. The characteristic length describes the region contributing to the major part of the lift force.

Equation (10) can be understood in the following simple picture. When the small particle moves close to a surface in a viscoelastic fluid, different shears are generated on the separated lower and upper hemispherical surfaces. At a small aspect ratio, h_0/r, the asymmetric shear rate for the upper and lower parts of the cylinder leads to the shear-induced first normal stress s_{xx} distributing unevenly. The first normal stress dominantly contributes to the lift force, and the dimensionless characteristic length scale, $(rh_0)^{0.5}$, corresponds to the determined region to produce the lift force. The flow in the thin gap region confined between the lower hemisphere and the flat substrate is analogous to the plane shear flow, coming up with a reasonable estimation of the first normal stress. Above all, inspired by Eq. (10), we finally suggest a formula of the lift force with a clear physical background as

$$f_{\text{lift}} = AWi\mu_p \frac{r^{0.5}}{h_0^{1.5}} \tag{11}$$

where A is a fitting coefficient as a correction from Eq. (10) due to its integration limited in the determined region. The dimensionless velocity u in Eq. (10) is equal to 1 for a convenient purpose during the simulation and thus does not appear in Eq. (11).

To understand Eq. (11) parallelly from the perspective of math, a general consideration of the scaling relationship includes the viscosities of the polymer and the solvent, the length scale and the kinetic characteristics of the system, and the Weissenberg number representing the interaction between the polymer elasticity and the system dynamics. First, the exponent of Wi is justified to take the value of 1.00 according to Eq. (6b), since the velocity contour and the shear rate-dependence elastic stress change very little in the ranges of $Wi(0.10\text{-}1.00)$, μ_p (μ_{p0} = 5 mPa·s - 20 mPa·s), as indicated in Fig. 2. Second, with respect to the ratio of the polymer and solvent viscosities, μ_p, its exponent is also justified to take the value of 1 due to the constitutive equation (Eq. (2)), indicating that the elastic component increases in the same degree in the situation that the relaxation time keeps constant. Third, for the length scale, it can be divided into a direct magnification factor of the system, R_0, which has been considered in Wi, and the geometric characteristics. The lift force should also be related to the distance between the cylinder and the substrate, h_0, and the size of the cylinder, r.

To validate Eq. (11) strictly, the numerical calculation is conducted to examine the lift force as a function of the parameters in a wider range, with Wi varying from 0.05 to 5.00, μ_{p0} varying from 5 mPa·s to 20 mPa·s, and the different combinations of r, h_0 listed in Table 2. And the lift force obtained by the simulation is strictly calculated using Eq. (7) by integrating the pressure around the cylinder.

Table 2 List of r, h_0 in simulation

r	h_0
16	3.0, 2.0, 1.5, 1.0
12	3.0, 2.0, 1.5, 1.0
8	3.0, 2.0, 1.5
6	3.0, 2.0, 1.5

Figure 3 shows the comparison between the results from the scaling expression ($f_{\text{lift-}c}$) and the results from the numerical simulation ($f_{\text{lift-}n}$) under various simulation conditions. In Fig. 3(a), the linear tendency is verified in the wide ranges of Wi, μ_{p0}. The best consistency between $f_{\text{lift-}c}$, $f_{\text{lift-}n}$ within the two steps is obtained with $A = 2.05$ (as marked in the solid black line), which is very close to the estimated value of ~2 obtained in Eq. (10). When $f_{\text{lift}} > 15$, the numerical simulation begins to depart slightly from the scaling expression with the constant coefficient $A = 2.05$. A correction of $A' = 1.73$ is given to draw the corresponding black dash line shown in Fig. 3. A better fitting is regained between the two results.

Moreover, Figs. 3(b), 3(c) show the zoom-in plots in linear scales at a fixed $h_0 = 1.5$ (Fig. 3(b)) and at a fixed $r = 12$ (Fig. 3(c)) with different values of Wi and different polymer viscosities at a constant fitting coefficient of $A = 2.05$. The viscosity ranging from 5 mPa·s to 20 mPa·s does not influence the accuracy of the scaling expression. The results of different values of Wi are drawn in different colors in both Figs. 3(b), 3(c). In Fig. 3(b), at fixed $h_0 = 1.5$, it can be seen that the scaling expression fits better with the results of the numerical expression with $A = 2.05$ for $Wi < 3$. With the increase of Wi, the difference between the two results increases as well. In Fig. 3(c), at fixed $r = 12$, a smaller h_0 / r also leads to a larger lift force, resulting in an increased departure between two results. Overally, in our simulation, when $Wi > 3$, $h_0 / r < 1/4$, the fitting coefficient of $A = 2.05$ in the scaling expression of Eq. (9) should be modified for better accuracy. Thus here, a value of $A' = 1.73$ is chosen.

Based on Eq. (11), we further obtain the dimensional equation of the lift force as follows

$$F_{\text{lift}} = A\lambda_1 \frac{U^2}{H_0^2} \mu_{p0} (RH_0)^{0.5} \tag{12}$$

To sum up, the lift force results from the asymmetric shear rate, which induces the non-zero integration of the first normal stress around the cylinder. In Eq. (12), $\lambda_1 U^2 / H_0^2 \mu_{p0}$ represents the first normal stress (S_{xx}) in a plane shear flow, and the term $(RH_0)^{0.5}$ is the dimensional characteristic length, which corresponds to the determined region for the lift force. A smaller aspect ratio, h_0 / r, will produce a larger lift force. Thus, Eqs. (11), (12) capture the main feature of the interaction between the particle and the surface, and they can be regarded as a uniform expression in the viscoelastic systems with wide ranges of the Weissenberg number and the viscosities of the polymer and the solvent.

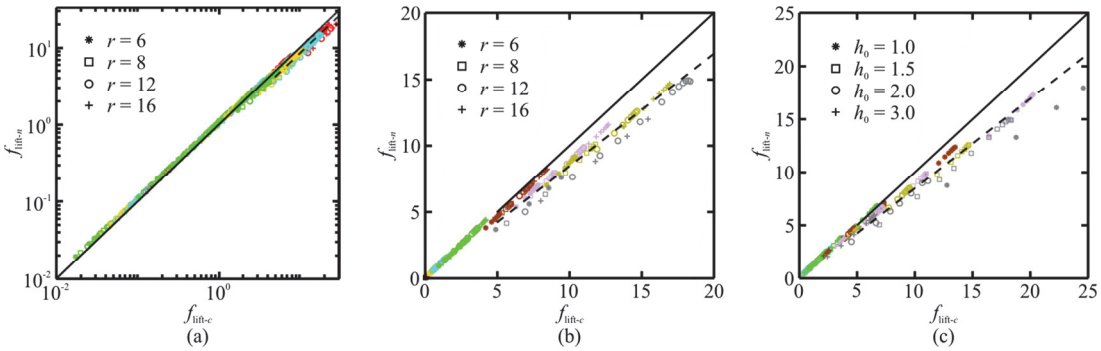

Fig. 3 (Color online) Lift forces from the scaling expression ($f_{\text{lift-}c}$) and numerical simulation ($f_{\text{lift-}n}$) under various simulation conditions. (a) Linear tendency shown by varying Wi from 0.05 to 5.00 and μ_{p0} from 5 mPa·s to 20 mPa·s. Symbols indicates the different combinations of h_0 (Red: $h_0 = 1.0$, blue: $h_0 = 1.5$, yellow: $h_0 = 2.0$, green: $h_0 = 3.0$). $f_{\text{lift-}c}$, $f_{\text{lift-}n}$ are shown consistency with $A = 2.05$ in the black solid line, and the black dash line for $Wi = 5.00$ with $A' = 1.73$. (b), (c) show the zoom-in plots of (a) in linear scales at a fixed $h_0 = 1.5$ (b) and at a fixed $r = 12$ (c), respectively (Red: $Wi = 0.05$, yellow: $Wi = 0.30$, blue: $Wi = 0.50$, green: $Wi = 1.00$, brown: $Wi = 2.00$, purple: $Wi = 3.00$, cyan: $Wi = 4.00$, gray: $Wi = 5.00$)

2.2 *Influence of Weissenberg number on lift force*

The simulation results shown in Fig. 3 already show that a constant fitting coefficient should be corrected to improve the accuracy when Wi increases. A larger Wi can change the velocity field significantly, making the derivative in Eqs. (5), (6) becomes less accurate. The influence of Wi on the pressure component p_e is elaborately discussed. Since there is no substrate to limit the flow above the upper surface of the cylinder, the pressure distributed around the upper surface should be much smaller than that distributed around the lower surface of the cylinder. Moreover, the pressure that contributes to the lift force is mainly in the determined region within the lower surface of the cylinder, indicating that the influence of the fluidic viscoelasticity on the pressure should be reflected mainly within the determined region. Thus, the pressure distributions within the determined region for different values of Wi ($\mu_{p0}=10\ \text{mPa}\cdot\text{s}$) are shown in Fig. 4(a). Due to the lift force, the total pressure of the viscoelastic fluid system should have an increment inside the determined region as compared to a viscous fluid system with only the pressure component of p_v. When $Wi>0.01$, the pressure at each position within the determined region shifts up left in different extents with the increase of Wi. When $Wi=1.00$, p_e is comparable with p_v. In this situation, the influence of p_e is strong enough to break the symmetry of the velocity contour. The asymmetry velocity contour will change the distribution of p_e. The pressure difference ($\delta p = p - p_v = p_e$) between the curves of the different viscoelastic fluids and the viscous fluid is shown in Fig. 4(b). It can be seen when $Wi<1.00$, the pressure difference is an even function, but when $Wi=1.00$, the pressure difference has lost its symmetry. It can be predicted that the symmetry will be worse when Wi increases, but the numerical results shown in Fig. 3 have verified that Eqs. (11), (12) can be applied in a range up to approximately $Wi=5.00$.

3. The lift force in a viscoelastic fluid over a soft substrate

The deformable soft surfaces widely exist in natural flows, especially in biological systems. The corresponding elasto-hydrodynamic force breaks the boundary symmetry and results in a lift force[1, 25]. In this section, a system with a rigid cylinder immersed in a viscoelastic fluid but moving near a soft substrate is investigated. The governing equations in consideration of the soft substrate contain the stress resulting from the deformation of the substrate. Here, we consider a linear elastic material whose deformation can be described with the Láme constants. The governing equation of the soft substrate is given by:

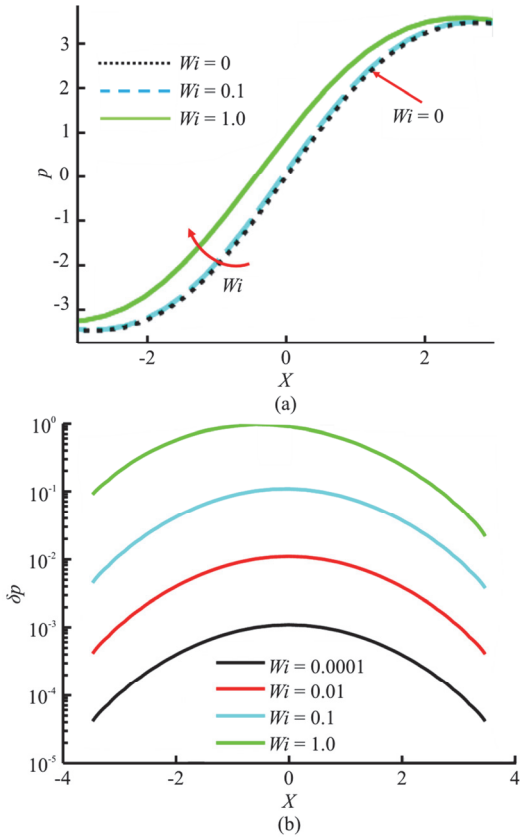

Fig. 4 (Color online) (a) Pressure distribution in different Weissenberg numbers ($\mu_{p0}=10\ \text{mPa}\cdot\text{s}$). Inlet: Blue mark line: determined region. $r=12$, $h_0=1.0$. (b) Pressure difference δp from (a)

$$\nabla\cdot\boldsymbol{\sigma}=0,\qquad \boldsymbol{\sigma}=G(\nabla\boldsymbol{D}+\nabla\boldsymbol{D}^{\mathrm{T}})+\beta\nabla\cdot\boldsymbol{D}\boldsymbol{I} \tag{13}$$

where $\boldsymbol{\sigma}$ is the stress tensor, $\boldsymbol{D}$ is the displacement field and G, β are the Láme constants.

Commonly, the viscosity of the viscoelastic fluids is several times of that of the water. For instance in the biology, the viscosity of the blood is 5 to 6 times of that of the water. Thus, to mimic a representative biological circumstance, the parameters in Table 3 are chosen in the simulation. Four different combinations of r, h_0 are simulated and the results are shown in Fig. 5(a). The blue dash line is the theoretical prediction of the lift force of a cylinder moving over a soft substrate immersed in a viscous fluid[25]. This theory was confirmed experimentally by Saintyves et al.[29] with a measurement of a terminal velocity of a cylinder freely rotating down a soft incline. It is seen that the lift force only induced by the

soft substrate is over three orders of magnitude smaller than that induced by the viscoelastic fluid with the rigid substrate or the soft substrate. Therefore, the influence of the soft substrate in a viscoelastic fluid is not a superposition of the lift forces arising from the soft substrate and the elasticity of the fluid. For a small Weissenberg number ($Wi < 0.01$), the soft substrate slightly enhances the lift force. For $r/h_0 = 6/3$, $r/h_0 = 16/3$, when Wi increases, the curves of the lift force with a soft or rigid substrate in a viscoelastic fluid are almost overlapped. The reason is that the deformation of the substrate is very tiny, for example, the maximum dimensionless deformation of the substrate (δ/L_0) at $Wi = 1.00$ for $r/h_0 = 6/3$ is 7.6×10^{-8}.

In the case $r/h_0 = 6/1.5$, when Wi approaches 1, the elasticity-induced lift force for a soft substrate is slightly larger than that for a rigid substrate, as indicated in Fig. 5(b). Figure 5(c) shows the pressure distribution in cases of soft and rigid substrates in a viscoelastic fluid and deformed substrate in case $r/h_0 = 6/1.5$. The absolute values of the peak pressures in the soft substrate case are slightly larger than its counterpart. The positive pressure increases more as compared to the negative one, leading to the overall increase of the lift force. Obviously, the pressure difference in two situations comes from different boun-

Table 3 Parameters of the simulation with a soft substrate

	Value
L_0/μm	10
r	6, 16
h_0	1.0, 1.5, 3.0
G /Pa	7.5×10^4
Viscosity of solvent, polymer/mPa·s	8.9, 40.0
Sweeping Wi	0.001-1.000
Velocity, u /(μm·s^{-1})	6
β /Pa	1.5×10^5

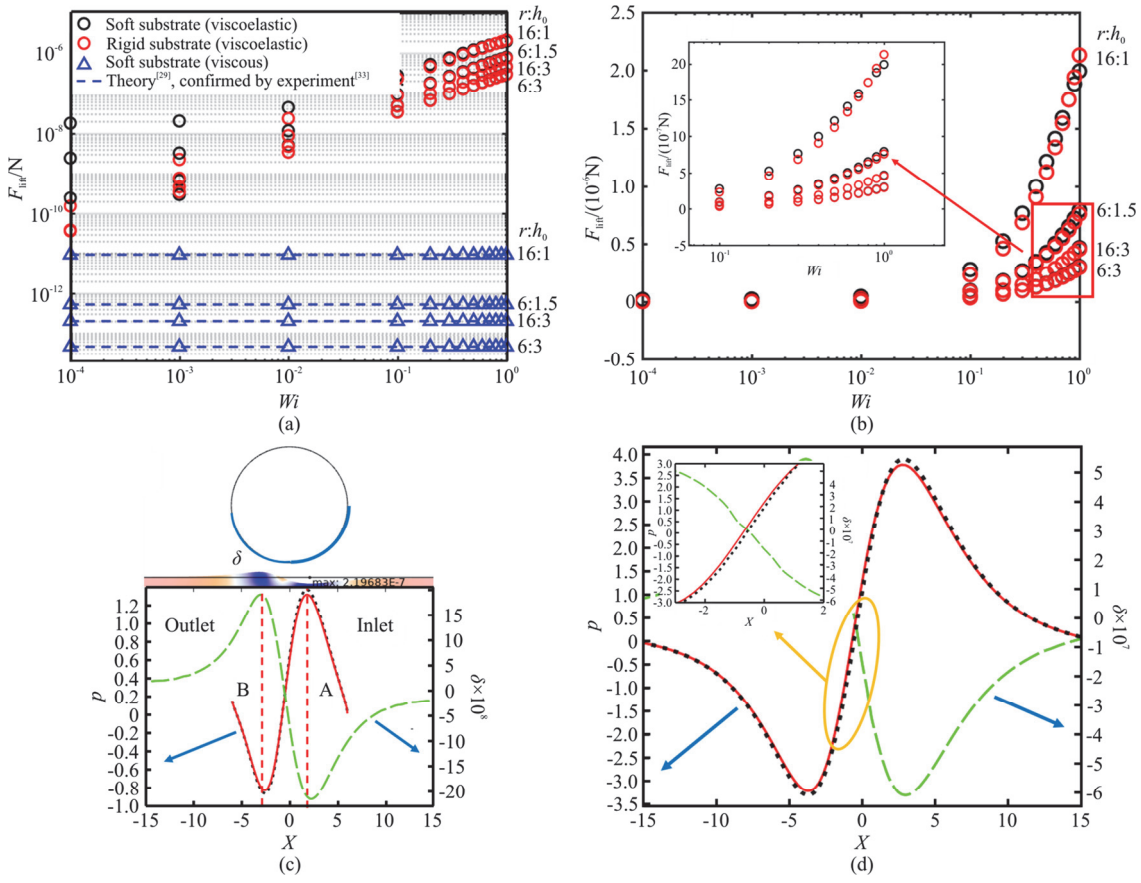

Fig. 5 (Color online) (a) Lift force varied with Wi in different simulated situations. Black circle: soft substrate and viscoelastic fluid, red circle: rigid substrate and viscoelastic fluid, blue triangle: soft substrate and viscous fluid, blue dash line: prediction of soft substrate and viscous fluid[25], confirmed in experiment[29]. (b) The same data in (a) plotted in a linear-log scale. Inset: magnification of red frame. Dimensionless pressure and substrate deformation in viscoelastic fluid (Black line: soft substrate, red line: rigid substrate, green line: deformation), (c) $r = 6$, $h_0 = 1.5$ and $Wi = 1.00$ and (d) $r = 16$, $h_0 = 1.0$ and $Wi = 1.00$

dary geometries. The deformation of the soft substrate is mainly determined by the pressure balanced by the viscous shear. The substrate in the inlet is sunken under the positive pressure, and in the outlet is extruded under the negative pressure. Around the line A in Fig. 5(c), the fluid flows upwards along the concave surface, and the cross-section area for the fluid to pass decreases, leading to the sudden increase of the pressure. Similarly, around the line B, the fluid flows downwards along the convex surface with a sudden increase of the cross-section area, leading to the release of the pressure.

In case $r/h_0 = 16/1$, the lift force for the rigid substrate exceeds that for the soft substrate at Wi over 0.8 in the viscoelastic fluid. In Fig. 5(d), regardless of the difference of the peak pressure, the pressure curve of the soft substrate between the two peaks shifts downwards, resulting in the overall decrease of the pressure. Such situation occurs due to a significant deformation that expands the gap so as to weaken the shear-induced first normal stress. A large ratio $r^{0.5}/h_0^{1.5}$ and a strong first normal stress induced by a large Wi enhance the deformation. In this situation the decreased pressure due to the negative deformation in the characterized region exceeds the increased pressure due to the boundary fluctuation. Therefore, by varying the boundary condition, the deformation of the substrate influences the pressure induced by the fluid elasticity.

Generally, the elastic parameters, G, of the soft material in nature vary in a wide range from kPa to MPa. In Fig. 6 we simulate the lift force for soft substrates of different values of softness. It is clear that, for the substrate of G in the range from 1.13 kPa to 1.02 MPa, the lift force in the viscoelastic system is always several order of magnitude larger than that in the viscous system for different combinations of r/h_0 at different Wi. It can be speculated that the lift force acting on the particle is mainly determined by the fluid viscoelasticity in the micro- and nanofluidics if both the viscoelastic fluid and the soft substrate exist. Even for a small Wi, for example, as in many biological systems, the value of Wi is around 10^{-3}-10^{-1}, the elasticity-induced lift force is still dominant.

4. Discussions

The polymer solution is a typical fluid with the viscoelastic behavior. The long polymer chains entangle to form a complex conformation chemically or/and physically, and thus exhibit the elasticity once being deformed. At the same time, the polymer in aqueous solution may also exhibit the shear-thinning behavior due to the entanglement stretched by the shear stress, such as the poly (ethylene oxide)[35], the polyvinylpyrrolidone[16], and the polyacrylamide[36] solutions. In such situation, Eq. (11) might overestimate the lift force, neglecting the shear-thinning effect. The shear-thinning rheological behavior is closely related with the polymer type, the weight, the concentration and the fabrication, and thus the convincing results usually come from experiments. The power-law model is the most common to be applied in the experiment data fitting. Based on the analysis in Section 2, the shear rate in the contact region can be evaluated to be constant. Since the elasticity-induced lift force is proportional to the relaxation time, thus a non-dilute polymer solution easily gives rise to a large lift force. Thus, approximately, with $m\dot{\gamma}^n = \mu_{p0} + \mu_{s0} \sim \mu_{p0}\ (-1 < n < 0)$, the lift force for the shear-thinning viscoelastic fluid is evaluated by using $F_{\text{lift}} \sim B\lambda_1 U^{2+n} R^{0.5} / H_0^{1.5+n}$, in which B is a fitting constant. Other sophisticated rheology models, concerning the thermo-, electrolyte and salt effect, can be considered similarly to be applied in different viscoelastic systems.

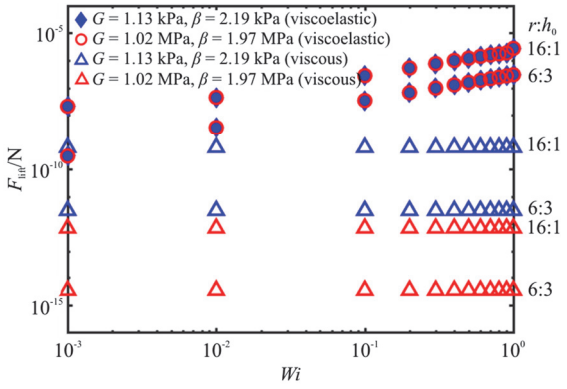

Fig. 6 (Color online) Lift force as a function of Wi over soft substrates with different values of softness

Besides, the development of the atomic force microscope (AFM) provides a direct way to measure the force on a moving spheric particle in the flow close to a boundary[31, 37]. In an advanced AFM investigation conducted by Zhang et al., they successfully measured the elastohydrodynamic lift force on a horizontally moving colloidal at the precision of 10^{-9} N and verified its theory[31]. Since the setup of our simulation is similar to the configuration of the AFM measurement, the present result offers an evaluation tool for the contributions from the elastic effect and the soft boundary in the complicated AFM measurement.

5. Conclusion

In this paper, we focus on a minimal model of the lift force acting on a rigid cylinder moving near a rigid

or soft substrate in a viscoelastic flow. We analyze how the mechanism of the lift force in the viscoelastic fluid system is affected by the system parameters. A scaling expression, including the viscosities of the polymer and the solvent, the length scale and the kinetic characteristics of the system, and Wi, is proposed for the cylinder moving over a rigid substrate in the viscoelastic fluid. This expression is confirmed to be well applicable in a wide range of the system parameters ($Wi < 5.00$, $\mu_{p0} < 20\ \mathrm{mPa \cdot s}$ and $h_0 / r < 0.5$). It is found that the lift force comes from the asymmetric first normal stress around the cylinder induced by the strong shear in the confined gap, and the strong shear, especially, concentrated within the characteristic length $(RH_0)^{0.5}$ around the gap between the cylinder and the substrate. Furthermore, the coupling case of the soft substrate and the viscoelastic fluid is considered. The deformation of the substrate influences the pressure induced by the fluid elasticity by changing the boundary condition. The lift force induced by the viscoelastic fluid dominates over that induced by the deformation of the soft substrate with G in the range from 1.13 kPa to 1.02 MPa, which demonstrates that the influence of the fluid elasticity is dominant in the hydrodynamics of the confined natural and biological situations when the Weissenberg number is not ignorable. Our findings provide a method of quantitatively calculating the lift force in the viscoelastic confinement and some insight for understanding the non-intuitive migration behaviors of microparticles in various biological and physiological applications.

Acknowledgement

The authors also thank Prof. Dong-shi Guan, Prof. Xu Zheng for useful discussion in manuscript writing.

References

[1] Rallabandi B., Oppenheimer N,, Zion M. Y. B. et al. Membrane-induced hydroelastic migration of a particle surfing its own wave [J]. *Nature Physics*, 2018, 14(12): 1211-1215.

[2] Feng J., Weinbaum S. Lubrication theory in highly compressible porous media: The mechanics of skiing, from red cells to humans [J]. *Journal of Fluid Mechanics*, 2000, 422: 281-317.

[3] Urzay J. Asymptotic theory of the elastohydrodynamic adhesion and gliding motion of a solid particle over soft and sticky substrates at low Reynolds numbers [J]. *Journal of Fluid Mechanics*, 2010, 653: 391-429.

[4] Mani M., Gopinath A., Mahadevan L. How things get stuck: Kinetics, elastohydrodynamics, and soft adhesion [J]. *Physical Review Letters*, 2012, 108(22): 226104.

[5] Snoeijer J. H., Eggers J., Venner C. H. Similarity theory of lubricated Hertzian contacts [J]. *Physics of Fluids*, 2013, 25(10): 101705.

[6] Pandey A., Karpitschka S., Venner C. H. et al. Lubrication of soft viscoelastic solids [J]. *Journal of Fluid Mechanics*, 2016, 799: 433-447.

[7] Segré G., Silberberg A. Radial particle displacements in Poiseuille flow of suspensions [J]. *Nature*, 1961, 189(4760): 209-210.

[8] Di Carlo D., Irimia D., Tompkins R. G. et al. Continuous inertial focusing, ordering, and separation of particles in microchannels [J]. *Proceedings of the National Academy of Sciences*, 2007, 104(48): 18892-18897

[9] Di Carlo D. Inertial microfluidics [J]. *Lab on a Chip*, 2009, 9(21): 3038-3046.

[10] Clime L., Morton K. J., Hoa X. D. et al. Twin tubular pinch effect in curving confined flows [J]. *Scientific Reports*, 2015, 5(1): 1-9.

[11] Segre G., Silberberg A. Behaviour of macroscopic rigid spheres in Poiseuille flow Part 2. Experimental results and interpretation [J]. *Journal of Fluid Mechanics*, 1962, 14(1): 136-157.

[12] Liu C., Xue C., Sun J. et al. A generalized formula for inertial lift on a sphere in microchannels [J]. *Lab on a Chip*, 2016, 16(5): 884-892.

[13] Liu C., Guo J., Tian F. et al. Field-free isolation of exosomes from extracellular vesicles by microfluidic viscoelastic flows [J]. *ACS Nano*, 2017, 11(7): 6968-6976.

[14] Feng J., Weinbaum S. Lubrication theory in highly compressible porous media: the mechanics of skiing, from red cells to humans [J]. *Journal of Fluid Mechanics*, 2000, 422: 281-317.

[15] Weissenberg K. The use of a trellis model in mechanics of homogeneous materials [J]. *Journal of the Textile Institute Transactions*, 1949, 40.

[16] Leshansky A. M., Bransky A., Korin N. et al. Tunable nonlinear viscoelastic "focusing" in a microfluidic device [J]. *Physical Review Letters*, 2007, 98(23): 234501.

[17] D'Avino G., Maffettone P. L. Particle dynamics in viscoelastic liquids [J]. *Journal of Non-Newtonian Fluid Mechanics*, 2015, 215: 80-104.

[18] Li G., McKinley G. H., Ardekani A. M. Dynamics of particle migration in channel flow of viscoelastic fluids [J]. *Journal of Fluid Mechanics*, 2015, 785: 486-505.

[19] Yu Z., Wang P., Lin J. et al. Equilibrium positions of the elasto-inertial particle migration in rectangular channel flow of Oldroyd-B viscoelastic fluids [J]. *Journal of Fluid Mechanics*, 2019, 868: 316-340.

[20] Paul S., Roy B., Banerjee A. Free and confined Brownian motion in viscoelastic Stokes–Oldroyd B fluids [J]. *Journal of Physics: Condensed Matter*, 2018, 30(34): 345101.

[21] Fetecau C., Fetecau C., Vieru D. On some helical flows of Oldroyd-B fluids [J]. *Acta Mechanica*, 2007, 189(1): 53-63.

[22] Fetecau C. Analytical solutions for non-Newtonian fluid flows in pipe-like domains [J]. *International Journal of Non-linear Mechanics*, 2004, 39(2): 225-231.

[23] Fetecau C. The Rayleigh–Stokes problem for an edge in an Oldroyd-B fluid [J]. *Comptes Rendus Mathematique*, 2002, 335(11): 979-984.

[24] D'Avino G., Greco F., Maffettone P. L. Particle migration due to viscoelasticity of the suspending liquid and its relevance in microfluidic devices [J]. *Annual Review of Fluid Mechanics*, 2017, 49: 341-360.

[25] Skotheim J. M., Mahadevan L. Soft lubrication: The elastohydrodynamics of nonconforming and conforming contacts [J]. *Physics of Fluids*, 2005, 17(9): 092101.

[26] Skotheim J. M., Mahadevan L. Soft lubrication [J]. *Physical Review Letters*, 2004, 92(24): 245509.

[27] Salez T., Mahadevan L. Elastohydrodynamics of a sliding, spinning and sedimenting cylinder near a soft wall [J]. *Journal of Fluid Mechanics*, 2015, 779: 181-196.
[28] Davies H. S., Débarre D., El Amri N. et al. Elastohydrodynamic lift at a soft wall [J]. *Physical Review Letters*, 2018, 120(19): 198001.
[29] Saintyves B., Jules T., Salez T. et al. Self-sustained lift and low friction via soft lubrication [J]. *Proceedings of the National Academy of Sciences*, 2016, 113(21): 5847-5849.
[30] Saintyves B., Rallabandi B., Jules T. et al. Rotation of a submerged finite cylinder moving down a soft incline [J]. *Soft Matter*, 2020, 16(16): 4000-4007.
[31] Zhang Z., Bertin V., Arshad M. et al. Direct measurement of the elastohydrodynamic lift force at the nanoscale [J]. *Physical Review Letters*, 2020, 124(5): 054502.
[32] Thomases B., Shelley M. Emergence of singular structures in Oldroyd-B fluids [J]. *Physics of Fluids*, 2007, 19(10): 103103.
[33] Isaacson E. Some periodic solutions of the two-dimensional Stokes-Oldroyd-B system with stress diffusion [R]. Berkeley, USA: University of California, Berkeley, 2012.
[34] Oldroyd J. G. On the formulation of rheological equations of state [J]. *Proceedings of the Royal Society of London. Series A. Mathematical and Physical Sciences*, 1950, 200(1063): 523-541.
[35] Ebagninin K. W., Benchabane A., Bekkour K. Rheological characterization of poly (ethylene oxide) solutions of different molecular weights [J]. *Journal of Colloid and Interface Science*, 2009, 336(1): 360-367.
[36] Jin L., Shangguan Y., Ye T. et al. Shear induced self-thickening in chitosan-grafted polyacrylamide aqueous solution [J]. *Soft Matter*, 2013, 9(6): 1835-1843.
[37] Leroy S., Steinberger A., Cottin-Bizonne C. et al. Hydrodynamic interaction between a spherical particle and an elastic surface: A gentle probe for soft thin films [J]. *Physical Review Letters*, 2012, 108(26): 264501.
[38] Huilgol R. R., Rhan-Thien N. Fluid mechanics of viscoelasticity: General principles constitutive modelling, analytical and numerical techniques [M]. Amsterdam, The Netherlands: Elsevier, 1997.

Appendix: Oldroyb-B viscoelastic fluid constitutive in a simple shear flow

The numerical simulations in this paper are conducted by using COMSOL Multiphysics in 2-D finite-element calculation. Oldroyb-B fluid, as one of the simplest, commonly used viscoelastic fluid, is chosen in the simulation to discuss the viscoelastic effect on the flow and the force acted on the cylindrical object in the flow. The constitutive equation of Oldroyb-B fluid has been given in Eqs. (2), (3), and the principles to transform to the dimensionless format are also used.

For the completeness, we design a simple shear flow case to validate the Oldroyb-B fluid constitutive in the modelling before we apply this modulus in the particle-laden fluid system. The model is introduced in Fig. A1, and the dimensionless simulation parameters are given as, the velocity of the upper surface movement $u=8$, and $D=4$, $\mu_p=\mu_{p0}/(\mu_{p0}+\mu_{s0})=0.41$ (μ_{p0} and μ_{s0} are the viscosities of the polymer and the solvent, respectively) and Weissenberg number from 0 to 1. The dimensionless stress tensor components in a simple shear flow can be given in an analytical way as[38]:

$$s_{xx}=2Wi\mu_p\left(\frac{u}{D}\right)^2,\quad s_{xy}=s_{yx}=\mu_p\left(\frac{u}{D}\right),\quad s_{yy}=0 \tag{A1}$$

With the output data, we can see in Fig. A2, Eq. (A1) can fit the simulation very well in all Weissenberg numbers.

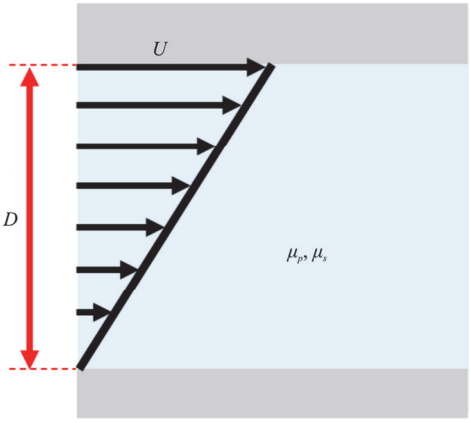

Fig. A1 (Color online) Modelling parameters

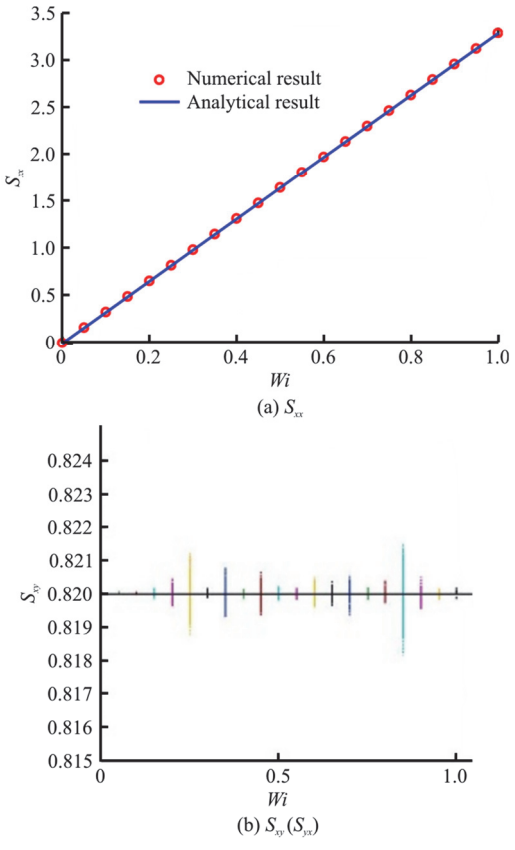

Fig. A2 (Color online) Stress tensor comparison